

# J|A|C|S

## A R T I C L E S

Published on Web 00/00/0000

### 3D Structure Determination of the Crh Protein from Highly Ambiguous Solid-State NMR Restraints

Antoine Loquet,<sup>‡</sup> Benjamin Bardiaux,<sup>#</sup> Carole Gardiennet,<sup>‡</sup> Christophe Blanchet,<sup>‡</sup>  
Marc Baldus,<sup>§</sup> Michael Nilges,<sup>#</sup> Thérèse Malliavin,<sup>#</sup> and Anja Böckmann\*<sup>‡</sup>

*Institut de Biologie et Chimie des Protéines, UMR 5086 CNRS Université Lyon 1, IFR128  
BioSciences Lyon-Gerland, 7, passage du Vercors, 69367 Lyon, France, Unité de  
Bio-Informatique Structurale, URA 2185 CNRS, Institut Pasteur, 25-28 rue du docteur Roux,  
F-75015 Paris, France, and Department of NMR-based Structural Biology, Max-Planck-Institute  
for Biophysical Chemistry, Am Fassberg 11, 37077 Göttingen, Germany*

Received October 19, 2007; E-mail: a.boeckmann@ibcp.fr

**Abstract:** In a wide variety of proteins, insolubility presents a challenge to structural biology, as X-ray crystallography and liquid-state NMR are unsuitable. Indeed, no general approach is available as of today for studying the three-dimensional structures of membrane proteins and protein fibrils. We here demonstrate, at the example of the microcrystalline model protein Crh, how high-resolution 3D structures can be derived from magic-angle spinning solid-state NMR distance restraints for fully labeled protein samples. First, we show that proton-mediated rare-spin correlation spectra, as well as carbon-13 spin diffusion experiments, provide enough short, medium, and long-range structural restraints to obtain high-resolution structures of this 2 × 10.4 kDa dimeric protein. Nevertheless, the large number of <sup>13</sup>C/<sup>15</sup>N spins present in this protein, combined with solid-state NMR line widths of about 0.5–1 ppm, induces substantial ambiguities in resonance assignments, preventing 3D structure determination by using distance restraints uniquely assigned on the basis of their chemical shifts. In the second part, we thus demonstrate that an automated iterative assignment algorithm implemented in a dedicated solid-state NMR version of the program ARIA permits to resolve the majority of ambiguities and to calculate a de novo 3D structure from highly ambiguous solid-state NMR data, using a unique fully labeled protein sample. We present, using distance restraints obtained through the iterative assignment process, as well as dihedral angle restraints predicted from chemical shifts, the 3D structure of the fully labeled Crh dimer refined at a root-mean-square deviation of 1.33 Å.

#### Introduction

The application of the two main analytical methods for 3D structure determination, X-ray crystallography, and liquid-state nuclear magnetic resonance spectroscopy (NMR), remains challenging for membrane proteins and protein fibrils. Even if membrane proteins can often be solubilized and sometimes be crystallized in the presence of detergents, their structural analysis in phospholipid bilayers is difficult by these methods. With regard to protein fibers, up to now only very short stretches of amino acids were amenable to crystallization, and only few studies exist on structural features of fibers from full-length proteins by classical approaches. Solid-state NMR (SSNMR) spectroscopy can address questions on structure, dynamics, and interactions of insoluble proteins (for recent reviews see references 1–4). The use of fully or extensively isotopically labeled proteins provides the opportunity to study these features using a single sample.

3D structure determination by NMR requires the measurement of long-range restraints in order to determine the fold of the protein. These restraints can be measured between nitrogen-15, carbon-13, and/or proton spins. Correlations between carbon-13 spins can be recorded directly by several types of multidimensional experiments. In SSNMR, polarization transfer is however dominated by the strong dipolar couplings between covalently bonded carbon spins. It has been shown recently that the resulting dipolar truncation is less severe in proton-driven spin-diffusion experiments,<sup>5</sup> so that the long-range ( $|i - j| > 4$ ) correlations which form the basis of protein fold determination can in principle be extracted from this type of spectra, even if the correlations observed largely originate from intra- and sequential connections. However, as the distribution of polarization within one amino acid proceeds fast compared to inter-residue polarization transfer, relayed mechanisms may have an important contribution to the observed cross-signals. This leads to less precision in the distance restraints derived from this type of spectra. Structure determination from carbon–carbon distances has been limited up to date to proteins labeled with strategic schemes, resulting in samples where most carbon-13 spins are neighbors to carbon-12 spins.<sup>6–9</sup>

<sup>‡</sup> UMR 5086 CNRS Université Lyon 1.<sup>#</sup> Institut Pasteur.<sup>§</sup> Max-Planck-Institute for Biophysical Chemistry.(1) McDermott, A. E. *Curr. Opin. Struct. Biol.* **2004**, *14*, 554–561.(2) Luca, S.; Heise, H.; Baldus, M. *Acc. Chem. Res.* **2003**, *36*, 858–865.(3) Böckmann, A. C. R. *Chim.* **2006**, *9*, 381–392.(4) Baldus, M. *Curr. Opin. Struct. Biol.* **2006**, *16*, 618–623.(5) Grommek, A.; Meier, B. H.; Ernst, M. *Chem. Phys. Lett.* **2006**, *427*, 404–409.

68 3D structures of small peptides have also been probed by  
69 selective recoupling schemes involving spin pairs. These  
70 methods can require however a large amount of selective  
71 experiments to be performed. Band-selective experiments have  
72 been introduced to selectively recouple spin-pairs in fully labeled  
73 peptides to determine multiple distances.<sup>10–13</sup> A high-resolution  
74 structure of the model tripeptide f-MLF-OH<sup>14</sup> and of the TTR-  
75 [105–115] peptide<sup>15</sup> could be determined using this approach.  
76 Developed for small peptides, this technique remains difficult  
77 to apply to larger systems, where the poor spectral dispersion  
78 presents a major obstacle for chemical-shift selection, and where  
79 multispin effects lead to complex correlations between polariza-  
80 tion exchange magnitude and distance.

81 Valuable information can also be obtained from measuring  
82 proton–proton distances. Recent work on spin-diluted proteins,<sup>16–18</sup>  
83 and also on fully protonated samples<sup>19</sup> at high spinning  
84 frequencies, points to the possibility to resolve and to directly  
85 detect them in near future. Another possibility, proposed by  
86 Baldus and co-workers in a series of experiments,<sup>20–22</sup> is to  
87 indirectly probe <sup>1</sup>H–<sup>1</sup>H interactions by a detection in 2D  
88 homonuclear (CHHC/NHHN), heteronuclear (NHHC), or 3D  
89 (CCHC/NHHCC) correlation spectra. In contrast to carbon  
90 correlations, where the dominant one-bond and two-bond  
91 correlations do not carry structural information, the large  
92 majority of correlations in proton-mediated spectra yield valu-  
93 able distance restraints. It has recently been demonstrated that  
94 proton-mediated, rare-spin detected correlation spectra yield  
95 enough restraints for the determination of the overall fold and  
96 the characteristic secondary structure elements for Ubiquitin<sup>23</sup>  
97 and Kalitoxin.<sup>24</sup>

98 One of the biggest challenges in both rare-spin and proton-  
99 mediated correlation experiments remains the unambiguous  
100 assignment of the peaks to distance restraints between two spins.  
101 All recent efforts for structure determination focused on  
102 relatively small proteins, while for larger proteins resonances

could only be assigned assuming homology models,<sup>23</sup> or in  
103 combination with strategic labeling schemes which reduce the  
104 number of resonances.<sup>8,9</sup> In solution NMR, the reduced line-  
105 width leads to a high accuracy of peak positions and experi-  
106 mental chemical shift values and allows, in the case of folded  
107 proteins of a size similar to the size of the catabolite repression  
108 HPr-like protein (Crh), to assign a large fraction of the 2D-  
109 NOESY or <sup>13</sup>C/<sup>15</sup>N-edited NOESY cross-peaks to a single and  
110 unique spin pair, the equivalent spins being considered as  
111 unique. In solid-state NMR, detection on rare spins (<sup>13</sup>C or <sup>15</sup>N)  
112 yields line widths of about 0.5 to 1 ppm. Compared to solution  
113 NMR, the number of isolated cross-peaks is greatly reduced,  
114 and the size of the chemical shift tolerance window must be  
115 increased. As a consequence, the majority of cross-peaks in  
116 <sup>13</sup>C–<sup>13</sup>C or <sup>15</sup>N–<sup>13</sup>C correlation spectra remain ambiguously  
117 assigned. In solution NMR, the use of ambiguous assignments<sup>25</sup>  
118 has been developed for the study of proteins larger than 10 kDa,  
119 as well as for the study of multimers, to account for the  
120 possibility of intramonomer and intermonomer cross-peak  
121 assignments.<sup>26</sup> The use of ambiguous distance restraints (ADRs)  
122 is widespread today to handle ambiguities in solution NMR (for  
123 applications see for example references 27–29). In the auto-  
124 mated structure calculation protocol ARIA,<sup>30</sup> an iterative  
125 procedure resolves ambiguous assignments by calculating sets  
126 of structures with ADRs, and applying a structure-based filter  
127 to discard the least probable assignments. The use of ADRs in  
128 the context of solid-state NMR data has been previously  
129 explored for the assignment of checkerboard-labeled proteins  
130 using a dedicated algorithm (SOLARIA).<sup>31</sup>

132 We use here as a model the 2 × 10.4 kDa Crh protein, which  
133 structure, determined by us using X-ray diffraction, shows a  
134 domain-swapped dimer.<sup>32</sup> For this protein, the structure deter-  
135 mination problem consists in the monomer structure determi-  
136 nation, as well as in the relative orientation of the two monomers  
137 to form the dimer. The latter presents a difficult problem in  
138 NMR,<sup>26,33,34</sup> and shall not be a subject discussed in this work;  
139 we here focus on the accurate determination of protein structure  
140 using SSNMR restraints.

141 The scope of the present work is twofold. First, we evaluate  
142 the information content of solid-state NMR proton-mediated,  
143 as well carbon-13, 2D correlation experiments and demonstrate  
144 that both contain enough distance restraints for the determination  
145 of a high-resolution 3D structure of the Crh model protein. In  
146 this first part, calculations are performed with distance restraints  
147 identified via the X-ray structure of the Crh dimer. In a second  
148 part, we evaluate whether de novo structure determination is  
149 possible from solid-state NMR data using the concept of

- (6) Hong, M.; Jakes, K. *J. Biomol. NMR* **1999**, *14*, 71–74.  
(7) Hong, M. *J. Magn. Reson.* **1999**, *139*, 389–401.  
(8) Castellani, F.; van Rossum, B.; Diehl, A.; Schubert, M.; Rehbein, K.; Oschkinat, H. *Nature* **2002**, *420*, 98–102.  
(9) Zech, S. G.; Wand, A. J.; McDermott, A. E. *J. Am. Chem. Soc.* **2005**, *127*, 8618–8626.  
(10) Ladizhansky, V.; Jaroniec, C. P.; Diehl, A.; Oschkinat, H.; Griffin, R. G. *J. Am. Chem. Soc.* **2003**, *125*, 6827–6833.  
(11) Ladizhansky, V.; Griffin, R. G. *J. Am. Chem. Soc.* **2004**, *126*, 948–958.  
(12) Jaroniec, C. P.; Filip, C.; Griffin, R. G. *J. Am. Chem. Soc.* **2002**, *124*, 10728–10742.  
(13) Rienstra, C. M.; Hohwy, M.; Mueller, L. J.; Jaroniec, C. P.; Reif, B.; Griffin, R. G. *J. Am. Chem. Soc.* **2002**, *124*, 11908–11922.  
(14) Rienstra, C. M.; Tucker-Kellogg, L.; Jaroniec, C. P.; Hohwy, M.; Reif, B.; McMahon, M. T.; Tidor, B.; Lozano-Perez, T.; Griffin, R. G. *Proc. Natl. Acad. Sci. U.S.A.* **2002**, *99*, 10260–10265.  
(15) Jaroniec, C. P.; MacPhee, C. E.; Bajaj, V. S.; McMahon, M. T.; Dobson, C. M.; Griffin, R. G. *Proc. Natl. Acad. Sci. U.S.A.* **2004**, *101*, 711–716.  
(16) Paulson, E. K.; Morcombe, C. R.; Gaponenko, V.; Dancheck, B.; Byrd, R. A.; Zilm, K. W. *J. Am. Chem. Soc.* **2003**, *125*, 15831–15836.  
(17) Chevelkov, V.; van Rossum, B. J.; Castellani, F.; Rehbein, K.; Diehl, A.; Hohwy, M.; Steuermagel, S.; Engelke, F.; Oschkinat, H.; Reif, B. *J. Am. Chem. Soc.* **2003**, *125*, 7788–7789.  
(18) Zhou, D. H.; Shea, J. J.; Nieuwkoop, A. J.; Franks, W. T.; Wylie, B. J.; Mullen, C.; Sandoz, D.; Rienstra, C. M. *Angew. Chem., Int. Ed.* **2007**.  
(19) Zhou, D. H.; Shah, G.; Cormos, M.; Mullen, C.; Sandoz, D.; Rienstra, C. M. *J. Am. Chem. Soc.* **2007**, *129*, 11791–801.  
(20) Lange, A.; Luca, S.; Baldus, M. *J. Am. Chem. Soc.* **2002**, *124*, 9704–9705.  
(21) Lange, A.; Seidel, K.; Verdier, L.; Luca, S.; Baldus, M. *J. Am. Chem. Soc.* **2003**, *125*, 12640–12648.  
(22) Heise, H.; Seidel, K.; Etzkorn, M.; Becker, S.; Baldus, M. *J. Magn. Reson.* **2005**, *173*, 64–74.  
(23) Seidel, K.; Etzkorn, M.; Heise, H.; Becker, S.; Baldus, M. *ChemBiochem* **2005**, *6*, 1638–1647.  
(24) Lange, A.; Becker, S.; Seidel, K.; Giller, K.; Pongs, O.; Baldus, M. *Angew. Chem., Int. Ed.* **2005**, *44*, 2–5.

- (25) Linge, J. P.; O'Donoghue, S. I.; Nilges, M. *Methods Enzymol.* **2001**, *339*, 71–90.  
(26) Nilges, M. *Proteins* **1993**, *17*, 297–309.  
(27) Luh, F. Y.; Archer, S. J.; Domaille, P. J.; Smith, B. O.; Owen, D.; Brotherton, D. H.; Raine, A. R.; Xu, X.; Brizuela, L.; Brenner, S. L.; Laue, E. D. *Nature* **1997**, *389*, 999–1003.  
(28) Aghazadeh, B.; Zhu, K.; Kubisaki, T. J.; Liu, G. A.; Pawson, T.; Zheng, Y.; Rosen, M. K. *Nat. Struct. Biol.* **1998**, *5*, 1098–1107.  
(29) Mott, H. R.; Owen, D.; Nietlispach, D.; Lowe, P. N.; Manser, E.; Lim, L.; Laue, E. D. *Nature* **1999**, *399*, 384–388.  
(30) Nilges, M.; Macias, M. J.; O'Donoghue, S. I.; Oschkinat, H. *J. Mol. Biol.* **1997**, *269*, 408–422.  
(31) Fossi, M.; Castellani, F.; Nilges, M.; Oschkinat, H.; van Rossum, B. J. *Angew. Chem., Int. Ed.* **2005**, *44*, 6151–6154.  
(32) Juy, M.; Penin, F.; Favier, A.; Galinier, A.; Montserret, R.; Haser, R.; Deutscher, J.; Böckmann, A. *J. Mol. Biol.* **2003**, *332*, 767–776.  
(33) Bewley, C. A.; Clore, G. M. *J. Am. Chem. Soc.* **2000**, *122*, 6009–6016.  
(34) Kuszewski, J.; Gronenborn, A. M.; Clore, G. M. *J. Am. Chem. Soc.* **1999**, *121*, 2337–2338.

ambiguous distance restraints (ADRs)<sup>26,35,36</sup> for automated 3D structure calculations. We show that nearly exclusively ambiguous <sup>1</sup>H–<sup>1</sup>H contacts detected on <sup>13</sup>C and <sup>15</sup>N spins in CHHC and NHHC spectra of the fully labeled <sup>13</sup>C/<sup>15</sup>N Crh protein can be automatically assigned in an iterative manner, and can be used to obtain a high-resolution 3D structure of this 2 × 10.4 kDa protein. Here, calculations are based on peak lists derived from the SSNMR spectra. This set of calculations comprises two steps: (i) ARIA is used to iteratively determine unambiguous restraints from the SSNMR peak lists; (ii) the structure is calculated using XPLOR-NIH using the unambiguous restraints determined by ARIA.

## 162 Materials and Methods

**163 Sample Preparation.** Crh was overexpressed with a C-terminal LQ-  
164 (6xHis) extension as described previously.<sup>37</sup> <sup>13</sup>C and <sup>15</sup>N-enriched Crh  
165 was prepared by growing bacteria in >98% <sup>13</sup>C, <sup>15</sup>N labeled medium  
166 (Silantes). The protein was purified on Ni-NTA agarose (QUIAGEN)  
167 columns followed by anion exchange chromatography on a Resource  
168 Q column.<sup>38</sup> Crh-containing fractions were dialyzed against 20 mM  
169 NH<sub>4</sub>HCO<sub>3</sub>. The protein was crystallized as described previously<sup>39</sup> in  
170 the presence of 20% PEG 6000 in a crystallization plate over a 2 M  
171 NaCl solution. The microcrystals resulting from about 20 mg of protein  
172 were centrifuged directly into a 4 mm CRAMPS rotor, and the rotor  
173 cap was sealed.

**174 NMR Spectroscopy.** NMR experiments were performed on a Bruker  
175 AVANCE DSX 500 MHz wide-bore spectrometer, equipped with  
176 double/triple resonance Bruker magic angle spinning (MAS) probes,  
177 at a spinning frequency of 11 kHz. All experiments were carried out  
178 between 0 and 5 °C sample temperature. A ramped cross-polariza-  
179 tion<sup>40,41</sup> was used in all experiments to transfer proton polarization to  
180 or from the <sup>13</sup>C or <sup>15</sup>N spins. High-power proton decoupling using the  
181 SPINAL-64 decoupling scheme<sup>42</sup> was applied during evolution and  
182 detection periods. The relaxation delay between scans was 2.5 s.  
183 Proton–proton contacts were encoded using two-dimensional (<sup>13</sup>C, <sup>13</sup>C)  
184 (CHHC) or (<sup>15</sup>N, <sup>13</sup>C) (NHHC) correlation experiments.<sup>20,21,43</sup> The 2D  
185 CHHC correlation spectrum was recorded using a first <sup>1</sup>H to <sup>13</sup>C 1 ms  
186 cross-polarization (CP) followed by two short CP steps of either 125  
187 μs and 200 μs (<sup>1</sup>H, <sup>1</sup>H) mixing time. Acquisition times were 15 ms in  
188 *t*<sub>2</sub> and 7.9 ms in *t*<sub>1</sub>, respectively, corresponding to a total acquisition  
189 time of 46 h. The spectral width was 350 ppm in the acquisition  
190 dimension and 90 ppm in the indirect dimension, centered in the  
191 aliphatic region. The <sup>1</sup>H rf field during SPINAL-64 decoupling and  
192 CP was set to 71 and 56 kHz, respectively. The <sup>13</sup>C rf field during CP  
193 was 34 kHz. The 2D NHHC correlation spectrum was recorded using  
194 a first <sup>1</sup>H to <sup>15</sup>N transfer of 900 μs. The subsequent CP contact times  
195 *t*<sub>NH</sub> and *t*<sub>CH</sub> were, respectively, 200 and 100 μs long. A proton mixing  
196 time of 100 μs was chosen. Acquisition times were 30 ms in *t*<sub>2</sub> and  
197 10.5 ms in *t*<sub>1</sub>. The total acquisition time was 35 h. The spectral widths  
198 in the <sup>13</sup>C and <sup>15</sup>N dimensions were 350 and 60 ppm, respectively. The

<sup>1</sup>H decoupling power was set to 71 kHz. The rf field strengths for <sup>15</sup>N 199  
and <sup>13</sup>C during CP were 38 and 34 kHz, respectively. 200

For the DARR<sup>44</sup> spectrum, a ramped CP<sup>40,41</sup> of 1 ms was used to 201  
transfer proton polarization to the <sup>13</sup>C spins. High power proton 202  
decoupling using the SPINAL-64 decoupling scheme<sup>42</sup> was applied 203  
during evolution and detection periods. The relaxation delay between 204  
scans was 2.5 s. During the mixing time of 200 ms, the radio frequency 205  
field on the proton channel matched the spinning frequency (11 kHz). 206  
Acquisition times were 20 ms in *t*<sub>2</sub> and 7.3 ms in *t*<sub>1</sub>, respectively, 207  
corresponding to a total acquisition time of 21 h. The spectral width 208  
was 250 ppm in both dimensions. 209

**210 Prediction of Dihedral Angle Restraints.** The TALOS<sup>45</sup> software  
211 was used to predict torsion angles from N, Cα, Cβ, and C′ chemical  
212 shifts.<sup>39</sup> Dihedral angle predictions for 56 out of 85 residues were  
213 considered as “good” by TALOS and used as dihedral angle restraints  
214 with error margins given by the program.

**215 Structure Calculations with SSNMR Distance Restraints Identif-**  
**216 ied Using the X-ray Structure.** <sup>1</sup>H–<sup>1</sup>H and <sup>13</sup>C–<sup>13</sup>C distance restraints  
217 were identified using the X-ray crystallographic structure of Crh as a  
218 homology model. Restraints for proton–proton distances were identified  
219 in proton detected, <sup>13</sup>C/<sup>15</sup>N spin detected experiments (CHHC and  
220 NHHC). <sup>1</sup>H–<sup>1</sup>H restraints were defined by a common lower bound of  
221 1.8 Å, a target distance of 3.5 Å for proton–proton distances identified  
222 in the NHHC spectrum, and 3.8 Å for distances identified in the CHHC  
223 spectrum, with a common upper bound of 5.0 Å. No distance classes  
224 were established, as suggested by our previous analysis of the  
225 correlation between polarization transfer build-up curves and distances  
226 measured on the Crh X-ray structure.<sup>46</sup> <sup>13</sup>C–<sup>13</sup>C distance restraints were  
227 identified in the DARR experiment, and bounds for these restraints  
228 were set to 2.5–7.0 Å.

Calculations of the monomer structure were realized using the 229  
program CNS (crystallography and NMR system) version 1.1.<sup>47</sup> A 230  
molecular dynamics simulated annealing protocol was used with torsion 231  
angles as internal degrees of freedom.<sup>48,49</sup> The structure calculation 232  
protocol consists of three stages: (i) 3000 steps of high-temperature 233  
torsion angle molecular dynamics at 50000 K; (ii) 5000 steps of slow- 234  
cooling annealing stage in torsion angle space from 50000 K to 0 K 235  
and (iii) 10 cycles of final conjugate gradient minimization, each cycle 236  
comprising 200 steps. 237

**238 Assignments of Ambiguous Distance Restraints by an Automated**  
**239 Iterative Process.** To assign cross-peaks from SSNMR spectra without  
240 the use of a homology model, we used a dedicated solid-state NMR  
241 version of the program ARIA 2.2, which can be obtained from Michael  
242 Nilges (nilges@pasteur.fr).

As in CHHC and NHHC experiments proton–proton interactions 243  
are indirectly detected on rare spins, this SSNMR version of ARIA 244  
allows the use of <sup>13</sup>C and <sup>15</sup>N chemical shifts, encoding <sup>1</sup>H–<sup>1</sup>H contacts. 245  
Chemical shifts, as well as cross-peak lists from CHHC and NHHC 246  
spectra, were used as input for the program. Manual peak picking was 247  
realized using the program Sparky 3.1 (T. D. Goddard and D. G. 248  
Kneller, University of California). Additionally, a set of 25 intermono- 249  
mer distance restraints<sup>50</sup> previously identified in a uniformly but 250  
heterogeneously [<sup>13</sup>C;<sup>15</sup>N] labeled protein Crh was used in these 251  
calculations, as well as the dihedral angle restraints from TALOS. In 252  
the ARIA program, the ambiguity in peak assignments is handled 253

(35) Nilges, M. *J. Mol. Biol.* **1995**, *245*, 645–660.

(36) Junius, F. K.; O’Donoghue, S. I.; Nilges, M.; Weiss, A. S.; King, G. F. *J. Biol. Chem.* **1996**, *271*, 13663–13667.

(37) Galinier, A.; Haiech, J.; Kilhoffer, M. C.; Jaquinod, M.; Stulke, J.; Deutscher, J.; Martin-Verstraete, I. *Proc. Natl. Acad. Sci. U.S.A.* **1997**, *94*, 8439–8444.

(38) Penin, F.; Favier, A.; Montserret, R.; Brutscher, B.; Deutscher, J.; Marion, D.; Galinier, A. *J. Mol. Microbiol. Biotechnol.* **2001**, *3*, 429–432.

(39) Böckmann, A.; Lange, A.; Galinier, A.; Luca, S.; Giraud, N.; Juy, M.; Heise, H.; Montserret, R.; Penin, F.; Baldus, M. *J. Biomol. NMR* **2003**, *27*, 323–339.

(40) Metz, G.; Wu, X. L.; Smith, S. O. *J. Magn. Reson. Ser. A* **1994**, *110*, 219–227.

(41) Hediger, S.; Meier, B. H.; Ernst, R. R. *Chem. Phys. Lett.* **1995**, *240*, 449–456.

(42) Fung, B. M.; Khitrin, A. K.; Ermolaev, K. *J. Magn. Reson.* **2000**, *142*, 97–101.

(43) Heise, H.; Hoyer, W.; Becker, S.; Andronesi, O. C.; Riedel, D.; Baldus, M. *Proc. Natl. Acad. Sci. U.S.A.* **2005**, *102*, 15871–15876.

(44) Takegoshi, K.; Nakamura, S.; Terao, T. *Chem. Phys. Lett.* **2001**, *344*, 631–637.

(45) Cornilescu, G.; Delaglio, F.; Bax, A. *J. Biomol. NMR* **1999**, *13*, 289–302.

(46) Gardiennet, C.; Loquet, A.; Etkorn, M.; Heise, H.; Baldus, M.; Böckmann, A., submitted for publication.

(47) Brünger, A. T.; Adams, P. D.; Clore, G. M.; DeLano, W. L.; Gros, P.; Grosse-Kunstleve, R. W.; Jiang, J. S.; Kuszewski, J.; Nilges, M.; Pannu, N. S.; Read, R. J.; Rice, L. M.; Simonson, T.; Warren, G. L. *Acta Crystallogr., D* **1998**, *54*, 905–921.

(48) Rice, L. M.; Brünger, A. T. *Proteins* **1994**, *19*, 277–290.

(49) Stein, E. G.; Rice, L. M.; Brünger, A. T. *J. Magn. Reson.* **1997**, *124*, 154–164.

(50) Etkorn, M.; Böckmann, A.; Lange, A.; Baldus, M. *J. Am. Chem. Soc.* **2004**, *126*, 14746–14751.

through the use of ambiguous distance restraints (ADR).<sup>30</sup> As the Crh protein is a homodimer, ambiguous distance restraints were also used to deal with the ambiguity between intra- and intermonomer restraints, using an effective distance of  $D = [\sum^N (d_{\text{intra}}^{-6} + d_{\text{inter}}^{-6})]^{-1/6}$ , where  $d_{\text{intra}}$  and  $d_{\text{inter}}$  correspond to the intra- and intermonomer distance, respectively. During the Crh dimer calculations, a packing distance restraint was applied between the centers of mass of the monomers, and a pseudoenergy term, the noncrystallographic symmetry (NCS) restraint,<sup>43</sup> was used to keep the two monomer units superimposable by minimizing the atomic rmsd between the two monomer units which form the dimer. The 2-fold symmetry was enforced through distance symmetry restraints.<sup>26</sup> The CNS torsion angle dynamics protocol used in ARIA consists for each iteration in (i) 1000 steps of an initial high-temperature conformational search at 2000 K, followed by (ii) two cooling stages in which the temperature is linearly decreased from 2000 to 1000 K and then from 1000 to 50 K. Considering the high degree of ambiguity of the NMR-derived restraints,<sup>51</sup> we used slow cooling stages: 80000/64000 for the first run, and 60000/48000 for the second run.

No automated peak-picking routine is implemented in ARIA. Peak-picking was realized manually with the program SPARKY. The threshold used was 2 times the noise measured on the spectra. The iterative assignment of restraints is performed automatically by ARIA, starting from the peak list determined using SPARKY. At each iteration, each peak is converted to a distance restraint, which is the weighted sum of several contributions between isolated protons. During the iterative algorithm, each contribution is filtered by rejecting the systematically violated contributions. The input values of the algorithm are the tolerance added to the upper and lower bounds before checking that the contribution is violated (violation\_tolerance varying from 1000 down to 0.1 Å), the threshold to determine whether a restraint is violated (violation\_threshold = 0.5 Å), the threshold for the contribution weight (weight\_threshold varying from 1.0 down to 0.8), and the maximum number of contributions (max\_contributions = 25).<sup>52</sup>

**Structure Calculations from Unambiguous Restraints Determined Using ARIA.** We used all unambiguous restraints assigned in the last iteration of the ARIA run as input for a final 3D structure calculation round using XPLOR-NIH.<sup>53</sup> Calculations started with the generation of a random monomer structure with good local geometry, followed by the duplication of the monomeric unit and a rotation of 180° around one of the internal axes to obtain a symmetric dimer. For each of the 200 random dimer structures generated, calculations proceeded through three stages: (i) a high-temperature searching phase at 2000 K (40000 steps), (ii) an annealing stage from 2000 to 100 K in temperature steps of 50 K and (iii) a final gradient minimization of 500 cycles of Powell minimization. During the Crh dimer calculations, a pseudoenergy term, the noncrystallographic symmetry (NCS) restraint,<sup>43</sup> was used to keep the two monomer units superimposable by minimizing the atomic rmsd between the two monomer units which form the dimer. The 10 lowest-energy conformers, as well as the NMR restraint data file, were deposited to the Protein Data Bank (PDB id: 2RLZ).

**Analysis of Obtained Structures.** The 10 selected conformers were aligned on the backbone atoms using MOLMOL 2K.2.<sup>54</sup> The software PROCHECK<sup>55</sup> was used to analyze the quality of the obtained conformers. The number of violations larger than 0.5, 0.3, and 0.1 Å, as well as the maximum violation and the rms of violations were also determined. We assessed the convergence by calculating the rmsd

between the conformers superimposed either on a hypothetical monomer (residues 2–12 of chain A, and 13–80 of chain B) or the complete dimer. We compared the distance between the centers of mass of the monomers, as well as the angles between the two monomers, to the corresponding values in the crystallographic structure.

## Results and Discussion

**Analysis of Proton and Carbon Contacts in the Crh Dimer.** We first evaluate the number and types of contacts found for different distance cut-offs in the Crh dimer, and compare them for protons and carbons, to assess which information content can be expected from the different spectra. Crh is 85 residues dimeric protein, with a tertiary structure formed by a four-stranded antiparallel  $\beta$ -sheet ( $\beta$ 1–4), and three  $\alpha$ -helices A, B, and C. In the hinge region, an intermolecular short  $\beta$ 1a-sheet is formed. Solid-state NMR sequential assignments and a threonon-based structural analysis of a microcrystalline form of the protein<sup>39</sup> have revealed that the dimeric domain-swapped form is present in this preparation as well. We thus used atomic coordinates from the 1.8 Å crystal structure (PDB entry: 1MU4<sup>32</sup>) to extract heavy-atom internuclear distances. Distances between protons were obtained by adding hydrogen atoms to the crystal structure using the MOLMOL program.<sup>54</sup> We used a cutoff of 5 Å for proton–proton distances<sup>20,21</sup> and of 7 Å for carbon–carbon distances.<sup>8</sup>

Each signal in carbon, as well as in heteronuclei detected proton correlation spectra, yield information about the spatial proximities between two spins. If spectra are crowded by short-range contacts carrying little structural information, identification of the medium- and long-range contacts becomes a difficult task. Their percentage consequently determines the amount of structural information that can be extracted. Figure 1a shows the distribution of distances involving either carbon or proton spins between short, medium and long-range as well as intraresidue contacts, with a distance cutoff of 3.5 and 5 Å for C–C, CH–HC, and NH–HC internuclear distances. For carbon spins, one bond and two bond contacts are highly dominant below 3.5 Å, as they represent more than 95% of potentially observable correlations in the C–C correlation spectra for this cutoff. The distribution for CH–HC contacts is different: even for a cutoff of 3.5 Å, long and medium range contacts account for a high percentage (about 40%). In NHHC spectra, the percentage of intraresidue contacts is even smaller, and a large number of sequential contacts are present. One should notice that, in contrast to carbon correlations, where one- and two-bond transfers proceed extremely fast within one residue and hamper distance calibration, in proton-mediated spectra even intraresidue contacts carry structural information.<sup>46</sup> For longer distance cut-offs (Figure 1a, right panel), the proportion of intraresidue/sequential and of medium/long-range contacts is similar for the three types of spectra, with slightly more long- and medium-range contacts still found in CHHC spectra. Figures 1b–d show a quantitative analysis of the number of contacts observed in the Crh X-ray structure as a function of the internuclear distance. For carbon correlations (Figure 1b), a large number of contacts (about 500) are present for one- and two-bond transfers. For proton contacts, intraresidue correlations dominate up to 2.5 in CHHC (Figure 1c) and 3 Å in NHHC (Figure 1d) experiments, and long- and medium-range contacts show an onset at shorter distances than for carbon spins (Figure 1b). The percentage (Figure 1e) and the total number of long-

(51) Fossi, M.; Oschkinat, H.; Nilges, M.; Ball, L. J. *J. Magn. Reson.* **2005**, *175*, 92–102.

(52) Habeck, M.; Rieping, W.; Linge, J. P.; Nilges, M. *Methods Mol. Biol.* **2004**, *278*, 379–402.

(53) Schwieters, C. D.; Kuszewski, J. J.; Tjandra, N.; Clore, G. M. *J. Magn. Reson.* **2003**, *160*, 65–73.

(54) Koradi, R.; Billeter, M.; Wüthrich, K. *J. Mol. Graphics* **1996**, *14*, 51–55.

(55) Laskowski, R. A.; MacArthur, M. W.; Moss, D. S.; Thornton, J. M. *J. Appl. Crystallogr.* **1993**, *26*, 283–291.

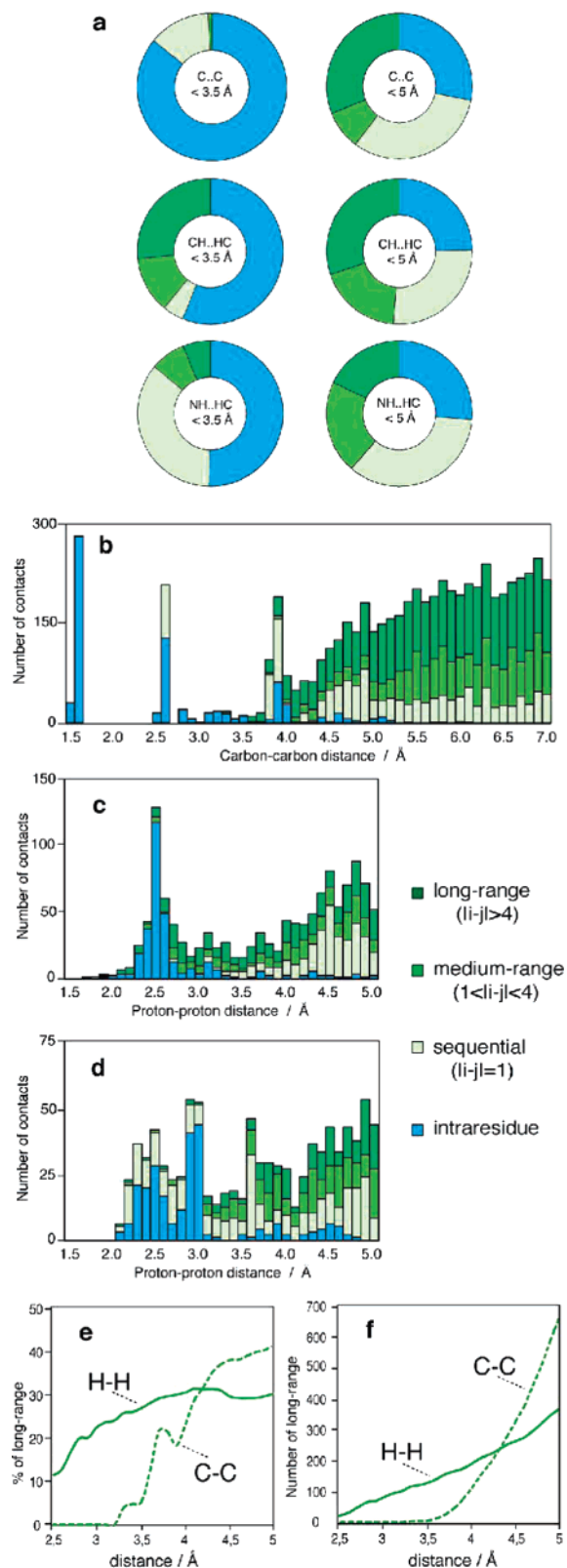


**Figure 1.** (a) Distribution between long-range (dark green), medium-range (green), sequential (light green), and intraresidue (blue) contacts involving carbon spins (C...C) and proton spins (CH...HC and NH...HC) in the Crh protein for distance cut-offs of 3.5 (left) and 5 Å (right). Number of contacts between carbon spin pairs (b), between proton spin pairs bonded to carbon atoms (c), and proton pairs with one proton bonded to a nitrogen spin and one proton bonded to a carbon spin (d), shown as a function of the internuclear distance in Å. (e) Fractions and (f) total numbers of long-range proton-proton and carbon-carbon contacts as a function of the distance in Å.

range contacts (Figure 1f) for carbon and proton correlations show that for distances smaller than 4 Å, proton contacts are dominant. For longer distances, the percentage of long-range contacts between protons increases only slightly; the total number of carbon contacts however increases rapidly. Nevertheless, for long distances, the precision of these contacts may be compromised by different factors like dipolar truncation, relayed polarization transfer, spectral crowding and relaxation; thus the most useful restraints arise from long-range contacts at short distances.

**Analysis of Distance Restraints Experimentally Observed in the SSNMR Spectra.** We first investigate whether the proton-proton and carbon-carbon distance restraints extracted from CHHC/NHHC<sup>20–22</sup> and DARR<sup>44,56,57</sup> spectra are sufficient to calculate high-resolution 3D structures of the Crh protein. This has been demonstrated using proton-mediated experiments for smaller molecules,<sup>23,24</sup> but no structures have yet been determined using carbon-13 distances measured in fully labeled proteins. We have recently shown for the Crh protein that CHHC and NHHC spectra contain high numbers of both local and long-range distance restraints.<sup>46</sup>

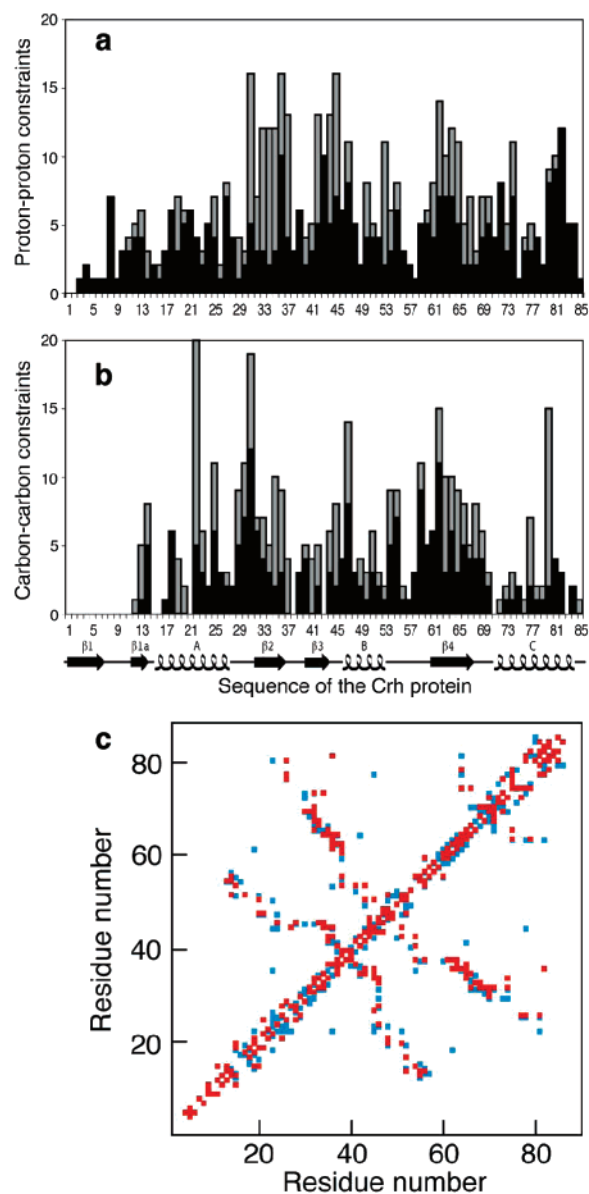
Using an assignment strategy based on the distances in the crystal structure, we prepared a list of <sup>1</sup>H-<sup>1</sup>H distance restraints based on proton-mediated, rare-spin detected spectra. The strategy consists in considering the cross-peaks for which only one assignment is possible among the <sup>1</sup>H-<sup>1</sup>H contacts with a distance cutoff of 5 Å, and within a chemical shift window of  $\pm 0.25$  ppm with respect to the Crh chemical-shift assignments. A total of 192 proton-proton distance restraints were extracted from the CHHC spectrum and the NHHC spectrum (see below), including 88 long-range restraints (Figure 2a). As here we only consider cross-peaks with one unique assignment possibility, this results in a lack of restraints for  $\beta$ 1-strand involved in the domain swap, for which the majority of cross-peaks could be intra- or intermonomeric. The same assignment strategy was applied to the DARR<sup>44,56,57</sup> spectrum (shown in Supplementary Figure S1 in the Supporting Information). The carbon-carbon restraints identified in the same manner as described above for the CHHC spectra are shown in Figure 2b. A total of 196 restraints, including 88 long-range restraints have been extracted from DARR spectrum, which is about the same number as the restraints extracted from the CHHC spectrum. In comparison to the CHHC spectrum, the DARR spectrum shows fewer restraints in the hydrophobic core of the protein, and particularly between the three  $\beta$ -strands. Interestingly, more contacts between helices A and C are observed in <sup>13</sup>C-<sup>13</sup>C correlation experiments than in proton-mediated experiments.

Figure 2c shows the contact plot of the restraints identified in the proton-mediated rare-spin detected experiments (red) and in the DARR experiment (blue). The graph indicates that the correlations present in these two experiments are able to connect the different secondary structure elements of the protein Crh, and also reveals the complementarities of the two approaches.

**Calculation of the Crh 3D Structure from SSNMR Unambiguous Restraints.** To evaluate whether the correlations extracted from the CHHC, NHHC, and the DARR spectra provide enough structural data for high-resolution 3D structure

(56) Takegoshi, K.; Nakamura, H.; Terao, T. *Chem. Phys. Lett.* **1999**, *307*, 295–302.

(57) Morcombe, C. R.; Gaponenko, V.; Byrd, R. A.; Zilm, K. W. *J. Am. Chem. Soc.* **2004**, *126*, 7196–7197.



**Figure 2.** Number of distance restraints identified as a function of the amino acid sequence for the Crh protein: intraresidue, sequential, and medium-range distance restraints are shown in black, long-range in gray. (a) Proton–proton distance restraints identified in the CHHC/NHHC spectra. (b)  $^{13}\text{C}$ – $^{13}\text{C}$  restraints identified in the DARR spectrum. (c) Contact plot of the distance restraints identified from CHHC and NHHC spectra (red) and the DARR spectrum (blue).

429 calculation of the Crh protein, we have used these as distance  
 430 restraints in molecular-dynamics-based structure calculations.  
 431 For the sake of simplicity we start out on one monomer unit of  
 432 this dimeric domain-swapped protein. We used different sets  
 433 of data to calculate 100 structures for the protein Crh: (i)  
 434 restraints from CHHC and NHHC spectra; (ii) restraints from  
 435 DARR spectra, and (iii) restraints both from CHHC, NHHC,  
 436 as well as DARR spectra. We calculated structures with and  
 437 without using the dihedral angle information predicted from  
 438 chemical shifts using the TALOS program.<sup>45</sup>

439 Figure 3 shows the 10 lowest-energy conformers calculated  
 440 from the different data sets. It is clear from the figure that  
 441 calculations based only on carbon–carbon restraints (Figure 3a)  
 442 or on proton–proton restraints (Figure 3c) are sufficient to  
 443 provide the right protein fold. Both data sets yield structures

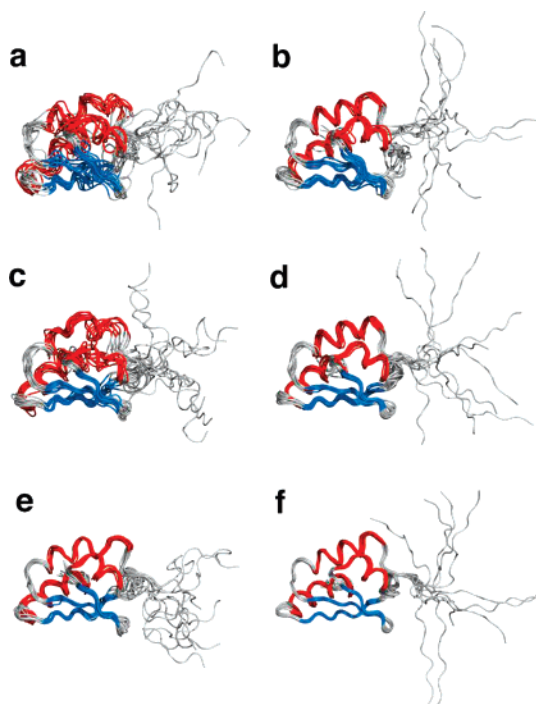


**Figure 3.** NMR ensemble of the 10 lowest-energy conformers calculated from (a) carbon–carbon restraints, (b) carbon–carbon restraints and TALOS dihedral angle predictions, (c) proton–proton restraints, (d) proton–proton restraints and TALOS dihedral angle predictions, (e) carbon–carbon and proton–proton restraints, (f) carbon–carbon, proton–proton restraints and TALOS dihedral angle predictions.

**Table 1.** Backbone RMSD Values for the Crh Monomer Structures Shown in Figure 3

Figure	restraints used	precision (Å) <sup>a</sup>	accuracy (Å) <sup>b</sup>
3a	$^{13}\text{C}$ – $^{13}\text{C}$	$2.4 \pm 0.1$	$2.5 \pm 0.3$
3b	$^{13}\text{C}$ – $^{13}\text{C}$ , TALOS	$1.3 \pm 0.1$	$1.5 \pm 0.1$
3c	$^1\text{H}$ – $^1\text{H}$	$1.9 \pm 0.2$	$2.5 \pm 0.2$
3d	$^1\text{H}$ – $^1\text{H}$ , TALOS	$1.0 \pm 0.1$	$1.4 \pm 0.1$
3e	$^1\text{H}$ – $^1\text{H}$ , $^{13}\text{C}$ – $^{13}\text{C}$	$1.0 \pm 0.1$	$1.6 \pm 0.1$
3f	$^1\text{H}$ – $^1\text{H}$ , $^{13}\text{C}$ – $^{13}\text{C}$ , TALOS	$0.6 \pm 0.1$	$1.3 \pm 0.1$

<sup>a</sup> Backbone rmsd between the 10 lowest-energy conformers. <sup>b</sup> Backbone rmsd between the average of the 10 lowest-energy conformers and the X-ray structure (PDB entry 1MU4<sup>32</sup>)

444 with an rmsd between the 10 lowest-energy conformers and  
 445 the X-ray structure of 2.5 Å (Table 1). As the  $^1\text{H}$ – $^1\text{H}$  distance  
 446 class is tighter than the one for  $^{13}\text{C}$ – $^{13}\text{C}$ , the precision of the  
 447 structures calculated from proton restraints is higher, with a  
 448 backbone rmsd of 1.9 Å (Figure 3c), compared to 2.4 Å for the  
 449 calculations from carbon restraints (Table 1). Using as input  
 450 both  $^1\text{H}$ – $^1\text{H}$  and  $^{13}\text{C}$ – $^{13}\text{C}$  distance restraints, the rmsd decreases  
 451 to 1 Å (Figure 3e), and the accuracy to 1.6 Å. The precision is  
 452 improved by the incorporation of TALOS dihedral angle  
 453 restraints, with a reduction of the backbone rmsd to ap-  
 454 proximately 1 Å for the calculations based on  $^1\text{H}$ – $^1\text{H}$  restraints  
 455 and to 1.3 Å based on  $^{13}\text{C}$ – $^{13}\text{C}$  restraints. For the calculations  
 456 including dihedral angle restraints and both  $^1\text{H}$ – $^1\text{H}$  and the  $^{13}\text{C}$ –  
 457  $^{13}\text{C}$  restraints, the backbone rmsd decreases to 0.6 Å. As the  
 458 TALOS dihedral angle prediction is most efficient for the  
 459 definition of local conformations, the gain in the accuracy of  
 460 the structure is smaller, with a decrease in rmsd from 1.6 to 1.3  
 461 Å (Table 1). A detailed analysis of the local rmsd of the different  
 462 calculations is given in the Supporting Information (Supple-  
 463 mentary Figure S2).

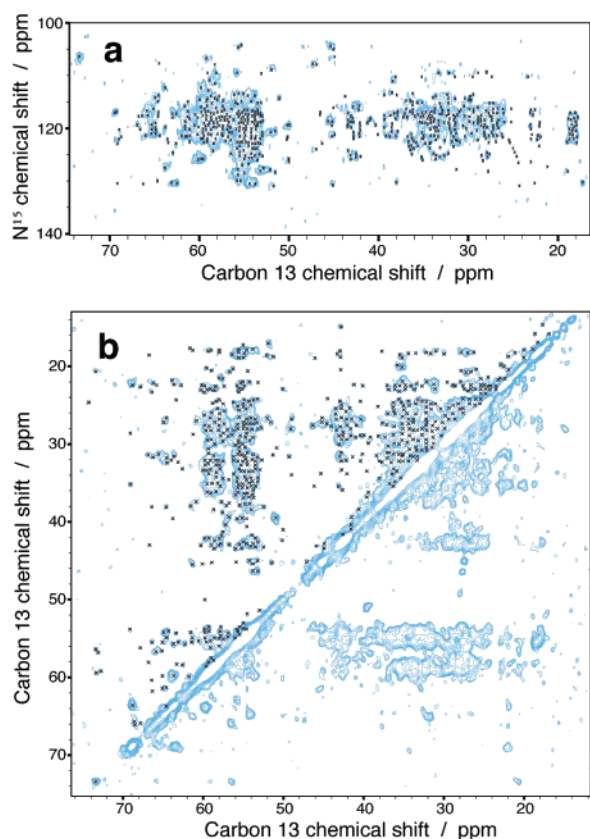


**Figure 4.** Peak-picking on spectra of the Crh protein: peaks picked (a) NHC spectrum (mixing time of 100  $\mu$ s), (b) CHHC spectrum (mixing time of 200  $\mu$ s).

464

#### Analysis of Spectral Ambiguities in the SSNMR Spectra.

465

In a second step we now resolve the high spectral ambiguities by using the concept of ambiguous distance restraints, which allows de novo protein structure determination, without the need of homology models. The iterative ARIA procedure<sup>58</sup> is used to assign the cross signals. As the default ARIA protocols are optimized for moderately ambiguous data, an optimization of certain parameters was necessary. Previous studies<sup>51,59</sup> have investigated the effects of critical parameters like the chemical shift tolerance, the maximum number of assignment possibilities allowed per peak, or the number of simulated annealing cooling steps for the solution NMR case. In the following we investigate the effect of these parameters on the efficiency of automated assignments of solid-state NMR data for the Crh protein. The data extracted from the solid-state NMR spectra consist of a peak list obtained by manual peak picking on CHHC/NHC spectra (Figure 4). The resulting peak list contains 1267 entries. For the following analysis, the Crh protein was treated as a hypothetical monomer, which means that ambiguities due to the distinction between intra- and intermonomer possibilities are not taken into account.

485

486

487

488

489

The choice of the chemical shift tolerance window has a substantial impact on the number of assignment ambiguities of the signals present in the peak list. A chemical shift tolerance window of  $\pm 0.1$  ppm (Figure 5a) leads to approximately 150 unambiguous cross-peaks, i.e., cross-peaks which can be

(58) Linge, J. P.; Habeck, M.; Rieping, W.; Nilges, M. *Bioinformatics* **2003**, *19*, 315–316.

(59) Fossi, M.; Linge, J.; Labudde, D.; Leitner, D.; Nilges, M.; Oschkinat, H. *J. Biomol. NMR* **2005**, *31*, 21–34.

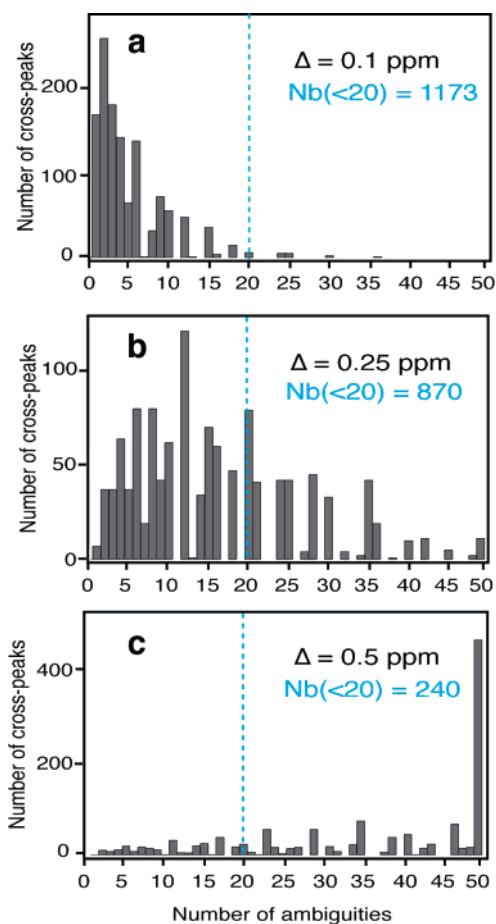


**Figure 5.** Influence of the chemical shift tolerance window on the number of ambiguities. Shown are histograms, for different chemical shift tolerance windows ( $a = 0.1$ ,  $b = 0.25$ ,  $c = 0.5$  ppm), of the number of proton–proton contacts as a function of possible assignments per cross-peak. The number of considered cross-peaks, with the number of assignment possibilities per peak set to 20 ( $N_b(<20)$ ) is given in each frame. Cross-peaks which represent more than 50 possible assignments are plotted at number of ambiguities = 50.

uniquely assigned on the basis of chemical shifts. For the spectra used here, a value of  $\pm 0.25$  ppm seems more realistic considering a typical line width of 0.5 to 1.0 ppm, and reduces the number of unambiguous cross-peaks to seven (Figure 5b). The average number of assignment ambiguities per peak is then 16.3, which leads to a set of highly ambiguous restraints for this medium-size protein. For comparison, in solution NMR studies of folded proteins of medium size, the  $^1\text{H}$  chemical shift tolerance is commonly set to values between 0.01 and 0.015 ppm in NOESY experiments, which typically leads to (i) a sufficient number of unambiguous restraints, which often allow a definition of the global fold of the protein, and (ii) a set of restraints showing only few ambiguities, often around 2–3, which can be easily assigned automatically by using the template structure calculated with the first set of restraints. The large average number of assignment ambiguities in the solid-state NMR case, combined with the small number of unambiguous restraints, illustrates well the difficulty to determine 3D structures of larger fully labeled proteins from SSNMR data without the use of automated iterative assignment software.

At a chemical shift tolerance window of 0.5 ppm (Figure 5c), no cross-peaks can be assigned unambiguously any more. A detailed analysis of the assignment statistics for different

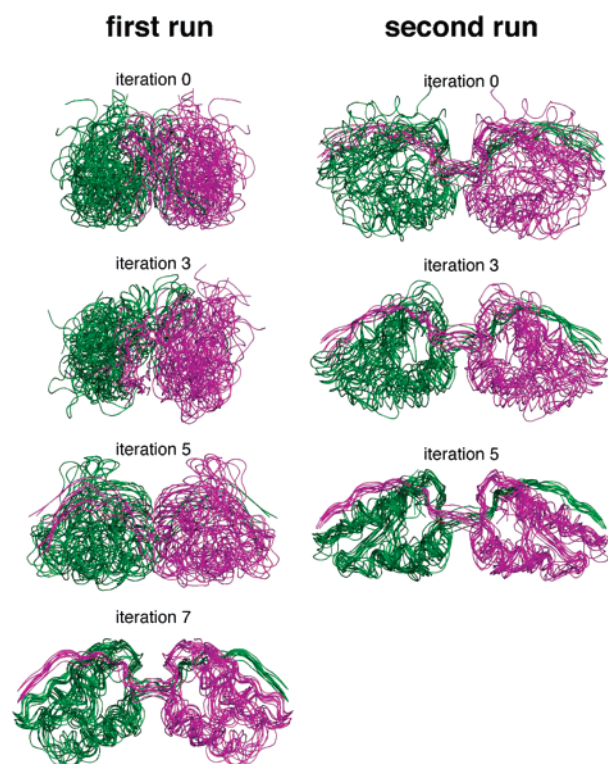


**Figure 6.** Comparison of conformers calculated in different iterations of ARIA runs: iterations 0, 3, 5, and 7 for the first run (left panel), iterations 0, 3, and 5 for the second run (right panel). Twenty-eight conformers are calculated for each iteration. The 10 lowest-energy conformers superimposed on the backbone atoms are shown.

chemical shift tolerance windows is given in the Supporting Information (Supplementary Figure S3).

**Automatic Assignments of Highly Ambiguous Restraints Using ARIA.** To determine the 3D structure of the Crh protein *without the need of a homology model*, we used the iterative assignment process implemented in ARIA program. The chemical shifts and the peak lists generated from the CHHC and NHHC spectra provided the input for the distance restraint assignments using ARIA. A chemical shift tolerance window of 0.25 ppm and a maximum number of assignment possibilities per peak of 25 (see Supplementary Figure S3 in the Supporting Information) were used, which results in a total number of 1002 cross-peaks, representing 32600 ambiguities, with an average number of  $2 \times 16.3$  ambiguities per peak, the factor of 2 taking into account the dimeric nature of the protein.

The left panel of Figure 6 shows the 10 lowest energy conformers obtained after iterations 0, 3, 5, and 7 from the first run of ARIA. The quality of the structures calculated for each iteration was evaluated with respect to the average number of ambiguities per cross-peak (Figure 7a), the number of unambiguous and ambiguous restraints (Figure 7b), as well as the precision and accuracy of the structures (Figure 7c). These Figures reveal the good correlation between the convergence of the conformers and the progress of the automated assignment.

The automated assignments performed by the ARIA program highly reduce the average number of ambiguities per peak in each iteration (Figure 7a), from 16.3 in iteration 0 to 2.5 in the last iteration. After the last iteration, 397 cross-peaks represent more than one possible assignment, with a reduced ambiguity level (2.5 possible assignment). The automated assignment procedure has achieved unambiguous assignments for 593  $^1\text{H}$ –

H J. AM. CHEM. SOC.

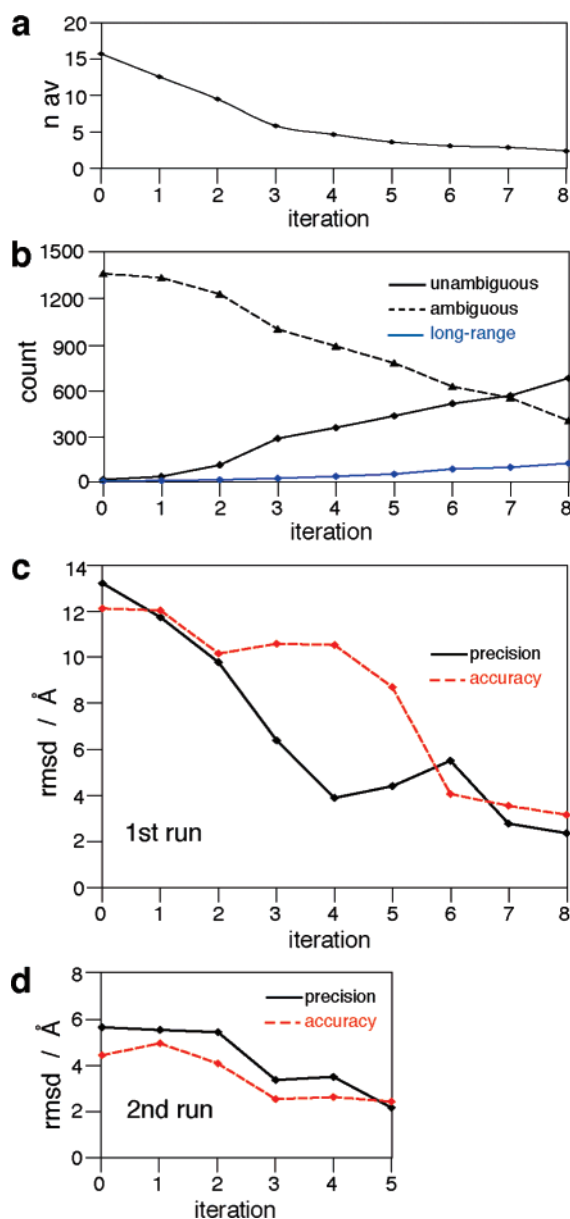


**Figure 7.** Analysis of the two runs performed using ARIA 2.2 for the structure calculations of the Crh dimer. Evolution as a function of the iteration number: (a) average number of possible assignments per cross-peak for the first run; (b) number of unambiguous, ambiguous, and long-range distance restraints for the first run; (c) backbone rmsd of the 10 lowest-energy conformers (precision) and backbone rmsd between the 10 lowest-energy conformers and the crystal structure (accuracy) for the first run; and (d) rmsd of the 10 lowest-energy conformers (precision) and rmsd between the 10 lowest-energy conformers and the crystal structure (accuracy) for the second run. Rmsd values were calculated for residues 2–81. In each iteration, 28 conformers were calculated, and the rmsd values is indicated for the 10 lowest-energy conformers.

$^1\text{H}$  contacts after the last iteration of the first run (Figure 7b), including 115 long-range restraints. Iteration 7 is the first iteration where the number of unambiguous restraints is higher than the number of ambiguous restraints. The precision of the structures increases with each iteration (Figure 7c), to reach a value of 2.8 Å for the iteration 8, and the rmsd decreases steeply during the five first iterations down to 4 Å.

To improve the convergence of the calculated structure, we have realized a second round of ARIA iterations. We used the 7 lowest-energy conformers obtained after iteration 8 of the first ARIA run as template structures to filter the possible assign-

544  
545  
546  
547  
548  
549  
550  
551  
552  
553  
554

555 ments in the second ARIA run. The same solid-state NMR data  
 556 was used for this second round (chemical shift and peak lists,  
 557 TALOS dihedral angle restraints and intermonomer restraints),  
 558 but the input of the template structures allowed to decrease the  
 559 number of possible assignments already during the first iteration.  
 560 We set the parameter of violation tolerance to 2 Å instead of  
 561 the standard value of 1000 Å used for the first iteration, and  
 562 reduced the number of iterations to 6. The right panel in Figure  
 563 6 shows the 10 lowest-energy conformers for iterations 0, 3,  
 564 and 5 of the second ARIA run. The addition of the template  
 565 structures highly increases the convergence of the first iteration  
 566 resulting in a precision of 5.6 Å (Figure 7d) compared to 13.2  
 567 Å at iteration 0 of the first run. As shown in Figure 6, the global  
 568 fold of the Crh protein is defined after the first iteration of the  
 569 second run, and the calculations converge to reach a precision  
 570 of 2.3 Å.

571 **Calculation of the Crh 3D Structure from the Unambiguous**  
 572 **Restraints Determined Using ARIA.** The automated  
 573 assignment procedure has achieved unambiguous assignments  
 574 for 643  $^1\text{H}$ – $^1\text{H}$  contacts in the last iteration of the second run,  
 575 including 131 long-range restraints. Iterative assignment has thus  
 576 been successful for about 65% of the initial 1002 peak entries.  
 577 In the ARIA protocol, the structures were calculated with both  
 578 unambiguous and ambiguous restraints. In the final structure  
 579 calculation realized using XPLOR-NIH, we used only the 643  
 580 unambiguous  $^1\text{H}$ – $^1\text{H}$  restraints assigned by ARIA, as well as  
 581 the TALOS dihedral restraints, to calculate a total of 200  
 582 conformers. A set of conformers was chosen on the basis of  
 583 the absence of distance violations  $>0.5$  Å. The 10 lowest-energy  
 584 conformers are shown in Figure 8a and c, and are compared to  
 585 the structure determined by X-ray crystallography (Figure 8b).  
 586 These 10 structures were analyzed using PROCHECK<sup>55</sup> and  
 587 show a good covalent geometry (Table 2); 74.2% of the residues  
 588 have backbone conformations in favorable regions and 20.6%  
 589 in allowed regions of the Ramachandran plot. The selected 10  
 590 conformers show a precision of 1.33 Å when superimposing the  
 591 backbone atoms for the dimer and an rmsd of 1.20 Å when  
 592 superimposing the heavy atoms in regular secondary structure  
 593 elements: the precision is improved with respect to the one  
 594 obtained after the second ARIA run. This improvement is  
 595 because only unambiguous distance restraints were considered  
 596 in this calculation round, as well as to the higher number of  
 597 conformers calculated. If we consider a hypothetical monomer  
 598 (residues 2–12 from chain A, and residues 13–80 from chain  
 599 B) (Figure 8c), the rmsd decreases to 0.84, and to 0.76 Å if  
 600 only regular secondary structure elements are taken into account.  
 601 The 10 selected conformers were deposited to the Protein Data  
 602 Bank (PDB id: 2RLZ). The backbone fold of the solid-state  
 603 NMR structure shows an accuracy of 2.89 Å with respect to  
 604 the single-crystal structure of the dimeric Crh protein (Figure  
 605 8a). The geometry of the obtained structure was also compared  
 606 to the geometry of the crystallographic dimer using the mean  
 607 distance of the monomer centers-of-mass, and the orientation  
 608 between the monomers, calculated as the angle formed by the  
 609 two vectors going from the center-of-mass of the interface region  
 610 (residues 10 to 15) to the center-of-mass of each monomer.  
 611 These two parameters display close mean values in the SSNMR  
 612 as well as in the crystallographic structures (Table 2). The  
 613 accuracy improves to 1.62 Å when considering the hypothetical  
 614 monomer, as shown in Figure 8c. Besides showing that the

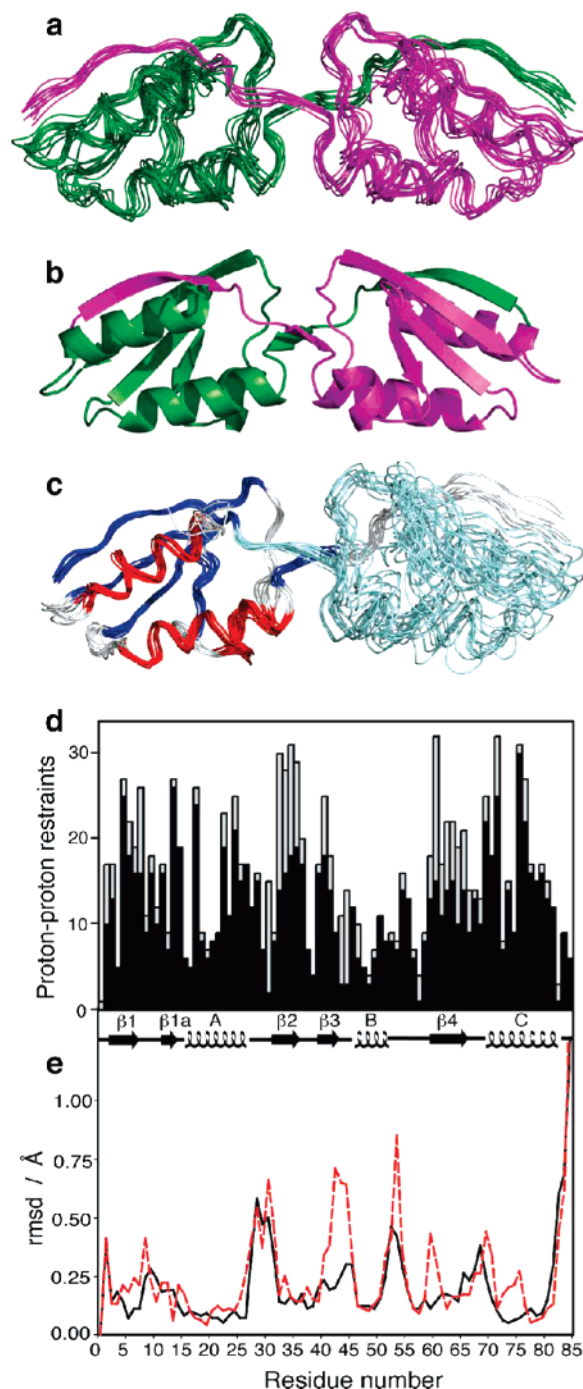


**Figure 8.** (a) Backbone ensemble of the 10 lowest-energy conformers of the dimer structure calculated from solid-state NMR data as described in the text; (b) dimer structure of Crh protein (PDB entry: 1MU4);<sup>32</sup> (c) backbone ensemble of the 10 lowest-energy conformers of the monomeric part of the dimer structure, with the superposition realized on one monomer (residues 2–12 from chain A, and residues 13–80 from chain B) (d) Proton–proton restraints used for the final structure calculations of the Crh dimer. Long-range restraints are shown in gray. (e) Local rmsd for the 10 lowest-energy conformers as a function of the primary sequence of Crh protein, calculated for the NMR conformers (black) and between the NMR and the crystal structure (red).

accuracy obtained for Crh is comparable to the one achieved 615  
 for other proteins using solid-state NMR methods (see below), 616  
 this also underlines that multimeric protein structure determina- 617  
 tion by NMR remains a challenge. 618

Figure 8d shows the distribution, as a function of the 619  
 sequence, of the unambiguous restraints used for the structure 620

**Table 2.** Structural Statistics for the 10 Lowest-Energy Conformers of the Crh Dimer Protein Calculated with XPLOR-NIH Using the Unambiguous Distance Restraints Assigned after the Second ARIA Run

no. of structures in the final set	10
no. of unambiguous distance restraints	
total	643
sequential ( $ i-j  = 1$ )	181
medium-range ( $1 <  i-j  < 5$ )	85
long-range ( $ i-j  > 4$ )	131
no. of backbone dihedral angle restraints	58
distance violations:	
$> 0.50 \text{ \AA}$	none
$> 0.30 \text{ \AA}$	$0.40 \pm 0.50$
$> 0.10 \text{ \AA}$	$2.20 \pm 1.30$
rmsd ( $\text{\AA}$ )	$0.012 \pm 0.005$
rmsd of the NMR ensemble <sup>a</sup> ( $\text{\AA}$ )	
monomer, backbone	$0.84 \pm 0.12$
monomer, SSE <sup>b</sup>	$0.76 \pm 0.09$
dimer, backbone	$1.33 \pm 0.23$
dimer, SSE	$1.20 \pm 0.24$
dimer, SSE all heavy atoms	$1.74 \pm 0.21$
rmsd $<10>$ versus X-ray structure <sup>d</sup> ( $\text{\AA}$ )	
monomer	1.62
dimer	2.89
deviation from idealized covalent geometry	
rmsd bond ( $\text{\AA}$ )	$0.0011 \pm 0.0007$
rmsd angles (deg)	$0.37 \pm 0.03$
rmsd impropers (deg)	$0.25 \pm 0.01$
Ramachandran data <sup>e</sup>	
residues in most favored region (%)	74.2
residues in allowed regions (%)	20.6
residues in generously allowed regions (%)	4.0
residues in disallowed regions (%)	1.2
Ramachandran data for SSE	
residues in most favored region (%)	89.6
residues in allowed regions (%)	8.7
residues in generously allowed regions (%)	0.8
residues in disallowed regions (%)	0.9
angle between the monomers (deg)	
final set of SSNMR structure	$164.3 \pm 4.0$
X-ray structure (1MU4)	164.8
distance versus the center of mass ( $\text{\AA}$ )	
final set of SSNMR structure	$22.1 \pm 0.7$
X-ray structure (1MU4)	20.7

<sup>a</sup> Calculated for residues 2–12 from chain A and residues 13–80 from chain B for the monomer, and residues 2–80 from both chains for the dimer. <sup>b</sup> SSE: secondary structure elements. <sup>c</sup>  $<10>$  represents the average for the 10 selected conformers. <sup>d</sup> Calculated on secondary structure elements between  $<10>$  and the X-ray structure (PDB entry 1MU4).<sup>32</sup> <sup>e</sup> From PROCHECK.<sup>55</sup>

621 calculation using XPLOR-NIH. Large numbers of long-range  
622 restraints are found in  $\beta$ -sheet regions, mainly due to numerous  
623  $^1\text{H}$ – $^1\text{H}$  side-chain contacts present in these secondary structure  
624 elements. The helical regions in the protein are less well defined,  
625 because the methyl and aromatic contacts, which would help  
626 to better define these regions, are difficult to detect in CHHC/  
627 NHHC experiments. Figure 8e shows the local rmsd of the 10  
628 lowest-energy conformers after the calculation with XPLOR-  
629 NIH. Low precision is observed in regions not corresponding  
630 to regular secondary structure elements, particularly the  
631 segment 27–32. The least restrained protein segments, which  
632 include helix B and beginning of loop 2 (residues 53–59),  
633 correspond to flexible regions of the protein<sup>60,61</sup> and show low  
634 accuracy.

### Comparison of the Convergence of the Crh Structure with That of Other Protein Structures Obtained from SSNMR Data.

635 The convergence of the Crh dimer structure calculated  
636 here was compared to the convergence of protein structures  
637 previously calculated from SSNMR data by calculating the  
638 backbone rmsd obtained on the NMR conformers. Two struc-  
639 tures have been determined from extensively labeled protein  
640 samples: SH3 (62 residues) and Ubiquitin (76 residues). The  
641 SH3 structure shows a precision of  $0.7 \text{ \AA}$  (calculated on the  
642  $\text{C}\alpha$  atoms in the secondary structure elements) and an accuracy  
643 of  $1.3 \text{ \AA}$  with respect to the crystal structure.<sup>8,62</sup> Ubiquitin shows  
644 a precision on the backbone atoms of about  $1.0 \text{ \AA}$ ; no accuracy  
645 is given.<sup>9</sup> Two structures were obtained for small fully labeled  
646 proteins by means of simple manual assignments: Kaliotoxin<sup>24</sup>  
647 (38 residues) and GB1<sup>18,63</sup> (56 residues). They show backbone  
648 rmsds of  $0.81$  and  $0.82 \text{ \AA}$ , respectively, and an accuracy of  $1.9$   
649  $\text{\AA}$ . The backbone rmsd of  $1.33 \text{ \AA}$  ( $1.20 \text{ \AA}$  on secondary structure  
650 elements) and the accuracy of  $2.89 \text{ \AA}$  obtained for the fully  
651 labeled Crh dimer (170 residues) is slightly higher than the  
652 values obtained for the above proteins; this increase can mainly  
653 be explained by the larger size of the protein, combined with  
654 the additional difficulty of the calculation of an elongated  
655 dimeric molecule. This is supported by the rmsd calculated for  
656 a hypothetical monomer, where the backbone rmsd for regular  
657 structure elements decreases to  $0.76 \text{ \AA}$ , and which shows an  
658 accuracy of  $1.62 \text{ \AA}$ , values which compare favorably to those  
659 of previously determined SSNMR structures.  
660

### Conclusion

662 We demonstrated how the structure of the fully  $^{13}\text{C}$ – $^{15}\text{N}$   
663 labeled dimeric form of the Crh protein can be derived using  
664 solid-state NMR techniques. We could show that proton and  
665 carbon distances can be extracted from 2D CHHC/NHHC as  
666 well as from DARR correlation spectra, and that the information  
667 content of both types of experiments is sufficient to calculate  
668 high-resolution structures. Carbon and proton restraints are  
669 complementary, and the combination of both, together with  
670 dihedral angles derived from chemical shifts, yields the highest  
671 resolution.  
672

673 We also could show, for the first time, how highly ambiguous  
674 proton-mediated, rare-spin detected solid-state NMR data sets  
675 of a fully labeled protein sample can be used for structure  
676 calculation through automated iterative assignments. The input  
677 of over 1000 cross-signals as ambiguous restraints, 25 inter-  
678 monomer restraints and chemical-shift derived dihedral angles  
679 yields a total of 643 unambiguously assigned distance restraints,  
680 including 131 long-range restraints. The Crh dimer structure  
681 calculated using this data shows a precision of  $1.33 \text{ \AA}$  and an  
682 accuracy with respect to the crystal structure of  $2.89 \text{ \AA}$ . Crh is  
683 the largest protein structure which has been determined so far  
684 from solid-state NMR data; our work shows that even complex  
685 structural features, like the dimeric and elongated nature of Crh,  
686 are not an obstacle to high-resolution structure determination  
687 by solid-state NMR.

688 This study is a further step toward the structure determination  
689 of insoluble proteins by the more general approach using fully  
690 labeled protein samples, and paves the way for the study of

(60) Favier, A.; Brutscher, B.; Blackledge, M.; Galinier, A.; Deutscher, J.; Penin, F.; Marion, D. *J. Mol. Biol.* **2002**, *317*, 131–144.  
(61) Giraud, N.; Böckmann, A.; Lesage, A.; Penin, F.; Blackledge, M.; Emsley, L. *J. Am. Chem. Soc.* **2004**, *126*, 11422–11423.

(62) Castellani, F.; van Rossum, B. J.; Diehl, A.; Rehbein, K.; Oschkinat, H. *Biochemistry* **2003**, *42*, 11476–11483.  
(63) Peng, X.; Libich, D.; Janik, R.; Harauz, G.; Ladizhansky, V. *J. Am. Chem. Soc.* **2007**.

691 larger molecules. For larger proteins, the use of 3D experiments  
692 is a means to increase spectral resolution and to considerably  
693 decrease the ambiguity level due to the additional frequency  
694 dimension; this is possible also by the use of higher magnetic  
695 fields, which equally benefit the limited signal-to-noise of  
696 proton-mediated rare-spin detected experiments. With higher  
697 resolution available, it is possible to decrease the chemical shift  
698 tolerance window, and room is left for the study of even larger  
699 molecules, without substantially modifying the ambiguity  
700 profile. The implementation of simultaneous iterative assign-  
701 ments of proton *and* carbon spectra, combined with the faster  
702 structure convergence using network anchoring,<sup>64</sup> should allow  
703 even higher resolution structures to be obtained.

(64) Herrmann, T.; Güntert, P.; Wüthrich, K. *J. Biomol. NMR* **2002**, *24*, 171–189.

**Acknowledgment.** This work has been supported by the 704  
Centre National de la Recherche Scientifique (PICS n° 2424), 705  
the Agence Nationale de Recherche (JC05\_44957, ANR-06- 706  
CIS6-005), the French ministry (ACI IMPBio), and the EU 707  
Network Extend-NMR. C.G. acknowledges a Claudie-Heigneré 708  
postdoctoral grant. 709

**Supporting Information Available:** The 2D DARR spectrum 710  
with assignments; analysis of the local rmsd for the structures 711  
calculated from unambiguous constraints; assignment 712  
statistics for different chemical-shift tolerance windows. This 713  
material is available free of charge via the Internet at 714  
<http://pubs.acs.org>. 715

JA078014T 716